

Visual-Semantic Graph Attention Networks for Human-Object Interaction Detection

Zhijun Liang, Junfa Liu, Yisheng Guan, and Juan Rojas

Guangdong University of Technology

Abstract

In scene understanding, machines benefit from not only detecting individual scene instances but also from learning their possible interactions. Human-Object Interaction (HOI) Detection infers the action predicate on a $\langle \text{subject}, \text{predicate}, \text{object} \rangle$ triplet. Contextual information has been found critical in inferring interactions. However, most works only use local features from single subject-object pair for inference. Few works have studied the disambiguating contribution of subsidiary relations made available via graph networks and the impact attention mechanisms have in inference. Similarly, few have learned to effectively leverage visual cues along with the intrinsic semantic regularities contained in HOIs. We contribute a dual-graph attention network that effectively aggregates contextual visual, spatial, and semantic information dynamically from primary subject-object relations as well as subsidiary relations through attention mechanisms for strong disambiguating power. We call our model: Visual-Semantic Graph Attention Networks (VS-GATs). We surpass state-of-the-art in the challenging HICO-DET dataset¹, including in long-tail cases that are harder to interpret. Code, video, and supplementary information is available at www.juanrojas.net/VSGAT.

1. Introduction

Human-Object Interaction (HOI) detection has recently gained important traction and has pushed forward machine’s abilities to understand the visual world. Generally, HOI detection starts with instance detection and continues with interaction inference as illustrated in Fig. 1(a). The goal is to infer an interaction predicate for the $\langle \text{subject}, \text{predicate}, \text{object} \rangle$ triplet. Whilst computer vision has experienced extraordinary advances in object detection

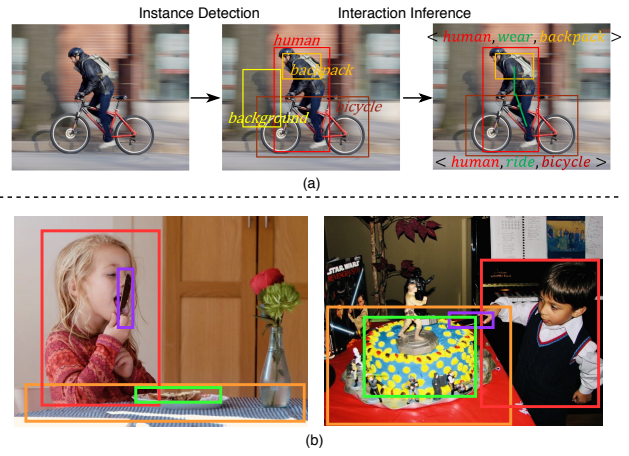


Figure 1. (a) HOI Detection: An object detector extracts subject and object proposals. Proposal features are used by an ‘interaction module’ to infer likely predicates. (b) How subsidiary relations facilitate HOI detection: On the left, with the features from $[\text{human-knife}]$, the model can easily infer “hold” and “lick” predicates for this tuple, while the message (from spatial features) from subsidiary relations $[\text{knife-table}]$ inhibits the model from choosing “cut”. On the right, if we just focus on the features from $[\text{human-cake}]$, the model may output similar scores for the “cut” and “light” predicates since they share similar embedding features. However, messages from subsidiary relations $[\text{human-knife}]$ and $[\text{knife-cake}]$ promote $\langle \text{human}, \text{cut}, \text{cake} \rangle$.

¹We also attach our comparable performance on V-COCO dataset in appendix.

Over time, researchers have exploited a variety of contextual cues including visual, spatial, semantic, interactivity, human pose, and functional approximation to better understand a scene [1, 3, 7, 8, 12, 18, 26, 34, 37]. Researchers have also used a variety of architectures including deep neural networks (DNNs) and graph neural nets (Sec. 2). But most works have only leveraged local-primary relations in the scene to infer interactions. Very recently graph attention nets [28] have been considered, however, they have been used with a limited set of contextual cues.

Under a graph-based structure, instance proposals yield graph nodes connected by edges. A primary relation is defined as the immediate human-object relation under consideration; whilst subsidiary relations are all other connections in the graph. In this manner, primary and subsidiary relations are relative. The key insight of this work is that leveraging various contextual cues from subsidiary relations have a strong disambiguating power in HOI detection. For example, in Fig. 1(b) consider the *[human-knife]* relation to be the primary relation on the left and the *[human-cake]* to be the primary relation on the right. On the left, this primary relation’s visual and spatial cues might predict hold or cut. But cues from the subsidiary relations *[knife-bread]*, *[human-table]* inhibit the system from choosing “cut”. On the right, the primary relation’s cues might predict cut or light as these actions share similarly embeddings. However, only when the system pays attention to the *[knife-cake]* and *[human-knife]* subsidiary contextual cues can it infer that “cut” is the right interaction. Additionally, HOIs also possess intrinsic semantic regularities that aid detection despite diverse scenes [22, 37]. For instance, semantic cues from *human* and *knife*, may help the model focus on the actions related to the *knife* instead of other actions like “ride”.

In this paper, we study the disambiguating power of subsidiary scene relations and intrinsic semantic regularities via a double Graph Attention Network that aggregates visual-spatial and semantic information in parallel. This graph-based attention network structure explicitly enables the model to leverage rich information by integrating and broadcasting information through the attention mechanism. Our work is the first to use dual attention graphs. We call our system: Visual-Semantic Graph Attention Networks (VS-GATs).

Our method begins by using instance detection (Sec. 3.2) as shown in Fig. 2. Instances yield bounding-boxes with visual features and semantic categories. From this, a pair of Graph Attention networks are created. The first graph’s nodes are instantiated from the bounding-box visual features; while the edges are instantiated from corresponding spatial features (Sec. 3.3.1). The second graph’s nodes are instantiated from word embedding features associated with corresponding visual nodes (see Sec. 3.3.2). An attention mechanism then updates the node features of each

graph and learning from primary and subsidiary contextual relations. A combined graph is created by concatenating both graph’s node updated features. Then inference is done through a readout step on box-paired subject-object nodes. Please note that the network uses attention to leverage primary and subsidiary contextual cues to gain additional disambiguating power. In so doing, cases that may not be properly disambiguated directly from primary relations, can be discerned via the additional information provided by the subsidiary relations. Besides, the learned semantic knowledge from semantic graph assist the model for better detection.

The proposed model is trained and tested in the challenging HICO-DET dataset [3] and surpasses state-of-the-art (SOTA) for the Full, Rare and Non-Rare categories with mAPs of **20.27**, **16.03** and **21.54** respectively. The results show the rich contextual information learned from appropriate integration of features through our novel dual-graph attention network improves inference even for samples with few training examples.

2. Related work

In this section, we present the related works by keying in on the architecture type: multi-streams neural network and graph neural network.

Multi DNN Streams with Various Contextual Cues A primary way to do HOI detection has been to extract visual features from instance detectors along with spatial information to instantiate multi-streams of DNNs. Each stream may contain information of detected human(s), objects, and perhaps some representation of interaction. A final fusion step is undertaken where individual inferences scores are multiplied to yield a final one [3, 7, 8]. Lu *et al.* [22] considered semantic information under the multi-stream DNN setting stating that interaction relationships are also semantically related to each other. Gupta *et al.* [12] and Wan *et al.* [34] emphasized a fine-grained layout of the human pose and leverage relation elimination or interactiveness modules to improve inference. Li *et al.* [18], include an interactiveness network that like Gupta *et al.* eliminates non-interactive edges. Visual, spatial, and pose features are concatenated and input into the interactiveness discriminator which finally outputs a detection classification. Peyre *et al.* [26] use the similar concept of visual analogies. They instantiate another stream using a visual-semantic embedding of the triplet resulting in a triagram. Analogies like functional approximation rely on similarity of function but in this case at a visual level. However, these works are limited to local features for inference, and do not consider subsidiary relations. In this work, we explore using graph structure network to take the subsidiary relations into account for learning rich contextual information to facilitate HOI detection.

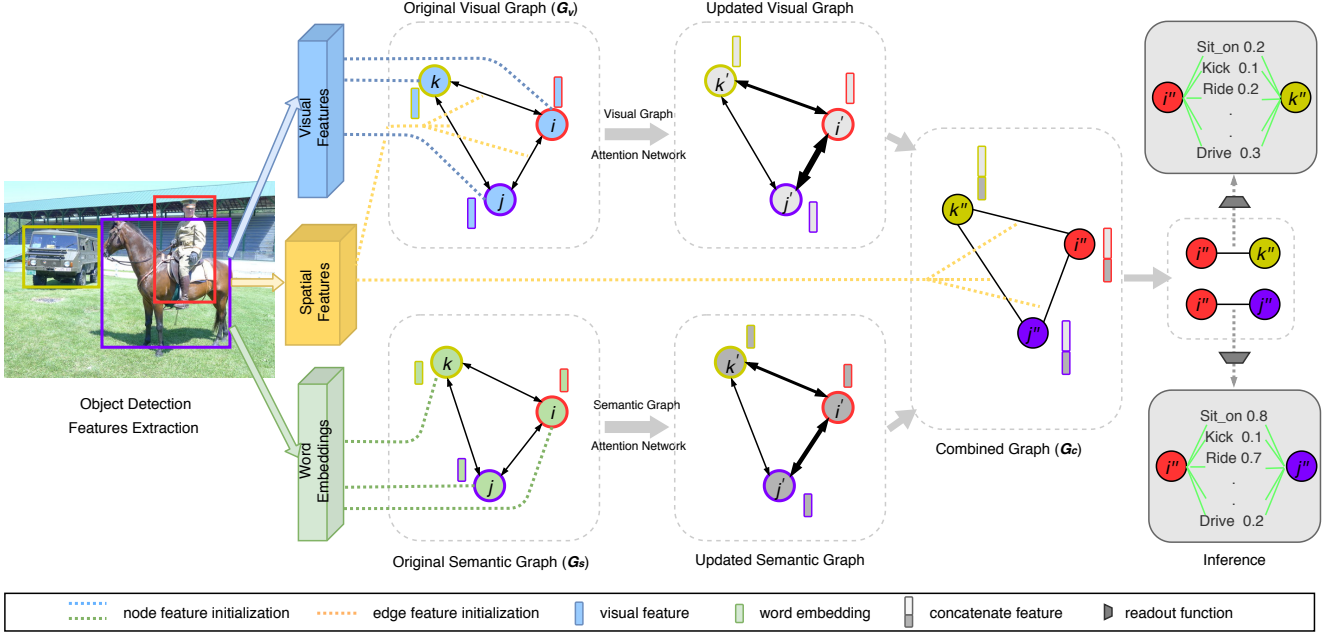


Figure 2. Visual-Semantic Graph Attention Network: After instance detection, a visual-spatial and a semantic graph are created. Node features are dynamically updated through attention network (Sec. 3.3). We combine these updated graphs and then perform a readout step on box-pairs to infer all possible predicates between one subject and one object.

Graph Neural Networks Graph Neural Networks (GNNs) [36] were first conceptualized as recurrent graph neural networks (RecGNNs) [10, 30]. RecGNNs learned a target node through neighbor information aggregation until convergence. Afterwards, Convolutional Graph Neural Networks (ConvGNNs) were devised under two main streams: spectral-based [2] and spatial-based approaches [24]. A node’s representation is created by aggregating self and neighboring features. ConvGNNs stack multiple graph layers to generate high-level node representations. Graph Attention Networks (GATs) were recently introduced by Velivckovic *et al.* [33]. GATs operate on graph structured data and leverage masked self-attentional layers. Nodes attend their neighbor’s features and dynamically learn edge-weight proportions with neighbors according to their usefulness.

GNNs have been used to model scene relations and knowledge structures. Yang *et al.* [40] proposed a Graph R-CNN network which contains a Relation Proposal Network to prune irrelevant relationships and an attentional graph convolution network to aggregate global context for scene graph generation. Sun *et al.* [31], do multi-person action forecasting in video. They use a RecGNN based on visual and spatio-temporal features to create and update the graph. Kato *et al.* [16] use an architecture that consists of one stream of convolutional features and another stream composed of a semantic graph for HOI classification. Learning on the concept of semantic regularities, Xu *et al.* [37]

similarly use a visual stream with convolutional features for human and object instances and a parallel knowledge graph for HOI detection.

To data, only Qi *et al.* [28] have used GAT architecture that consider subsidiary relations for HOI detection. Their graph parsing neural net (GPNN) creates nodes and edge from visual features. The graph structure is set by an adjacency matrix and message updates leverage attention mechanisms via a weighted sum of the messages of the other nodes. Finally, a node readout function is used for interaction inference. Our method is similar, but different. First, as illustrated in Fig. 2, instead of using single graph our model uses a novel parallel dual-attention graph architecture which also takes semantic cues into account. Furthermore, we identify spatial features as critical in the final inference step. Second, we also leverage a simpler but more effective node features updating mechanism. A final difference is that in [28], Qi *et al.* use a node readout function to *separately* infer actions for each node. We find it more reasonable to jointly infer actions with the combined features of the human and object; as such, we use an edge readout function (Eq. 14) to infer the interaction from the edges connected to the human. Overall, our model outperforms GPNN by a great margin on the HICO-DET dataset as shown in table 3.5.1.

3. Visual-Semantic Graph Attention Network

In this section, we first define graphs and then describe the visual and semantic instantiations, attention mechanisms, fusion step, inference, training, and implementation details.

3.1. Graphs

A graph G is defined as $G = (V, E)$ that consists of a set of V nodes and a set of E edges. Node features and edge features are denoted by \mathbf{h}_v and \mathbf{h}_e respectively. Let $v_i \in V$ be the i th node and $e_{i,j} = (v_i, v_j) \in E$ be the directed edge from v_i to v_j .

A graph with n nodes and m edges has a node features matrix $\mathbf{X}_v \in \mathcal{R}^{n \times d}$ and an edge feature matrix $\mathbf{X}_e \in \mathcal{R}^{m \times c}$ where $\mathbf{h}_{v_i} \in \mathcal{R}^d$ is the feature vector of node i and $\mathbf{h}_{e_{i,j}} \in \mathcal{R}^c$ is the feature vector of edge (i, j) . Fully connected edges imply $e_{i,j} \neq e_{j,i}$.

3.2. Contextual Features

Visual Features Visual features are extracted from subject and object proposals generated from a two-stage Faster-RCNN (ResNet-50-FPN) [14, 19, 29]. First, the RPN generates (hundreds) of subject and object proposals. Thus, for an image I , the i th human bounding-box b_h^i and the j th object bounding-box b_o^j are used to extract latent features from Faster-RCNNs last fully-connected layer ($FC7$ after the ROI pooling layer) to instantiate the visual graph (G_v) nodes as illustrated in Fig. 2.

Spatial Features Spatial features such as bounding box locations and relative locations are informative about the relationship that proposals have with each other [15, 27, 41, 42]. Spatial features are also useful to encode the predicate. Consider the “ride” predicate, then we can deduce that subject is above the object.

Given a pair of bounding boxes, their paired-coordinates are given by (x_i, y_i, x_j, y_j) and (x'_i, y'_i, x'_j, y'_j) and centres are denoted as (x_c, y_c) and (x'_c, y'_c) . Along with respective areas A and A' and an image area A^I of size (W, H) .

Spatial features can be grouped into (i) relative scale and (ii) relative position features. Bounding-box relative scale features s_{rs} are defined as:

$$s_{rs} = \left[\frac{x_i}{W}, \frac{y_i}{H}, \frac{x_j}{W}, \frac{y_j}{H}, \frac{A}{A^I} \right]. \quad (1)$$

Relative position bounding-box features s_{rp} are defined as:

$$s_{rp} = \left[\left(\frac{x_i - x'_i}{x'_j - x'_i}, \frac{y_i - y'_i}{y'_j - y'_i} \right), \log\left(\frac{x_j - x_i}{x'_j - x'_i}\right), \log\left(\frac{y_j - y_i}{y'_j - y'_i}\right), \frac{x_c - x'_c}{W}, \frac{y_c - y'_c}{H} \right]. \quad (2)$$

The relative position expression is similar to the bounding box regression coefficients proposed in [29], but two center scales are added to yield more obvious cues.

So, the set of spatial features s used in our architecture is the union of these sets $s = s_{rs} \cup s_{rp}$. Spatial features will be used to: (i) build the edges in the Visual graph (G_v) (ii) but also as part of the Combined Graph (G_c) in what amounts to a skip connection step in neural nets as illustrated in Fig. 2.

Semantic Features In this work, we use Word2vec embeddings as semantic features [23]. Word2vec takes a text corpus as input and produces latent word vectors \mathbf{w} as outputs. The latent representation retains semantic and syntactic similarity. Similar context is made evident through spatial proximity; indicating that words have mutual dependencies.

We use the publicly available Word2vec vectors pre-trained on the Google News dataset (about 100 billion words) [9]. The model yields a 300-dimensional vector for 3 million words and phrases and is trained according to [23]. All existing object classes in the HICO-DET dataset are used to obtain the Word2vec latent vector representations offline. These semantic features are used to instantiate the nodes in the semantic graph (G_s) as illustrated in Fig. 2.

3.3. Graph Attention Networks

GNN use the graph structure and node features \mathbf{X}_v to dynamically update the node vector representation [38]. An anchor node’s features are updated through aggregation—using neighboring features to update the anchor node. If time or multiple layers are involved, then after k aggregation iterations, a given node’s representation encodes updated structural information. The node aggregation features \mathbf{a}_{v_i} for node v_i is generically defined as:

$$\begin{aligned} \mathbf{a}_{v_i}^{(k)} &= f_{aggregate}^{(k)} \left(\left\{ \mathbf{h}_{v_j}^{(k-1)} : v_j \in \mathcal{N}_i \right\} \right) \\ \mathbf{h}_{v_i}^{(k)} &= f_{update}^{(k)} \left(\mathbf{h}_{v_i}^{(k-1)}, \mathbf{a}_{v_i}^{(k)} \right). \end{aligned} \quad (3)$$

Initially, $\mathbf{h}_{v_i}^{(0)} = \mathbf{X}_v$ and \mathcal{N}_i is the set of nodes adjacent to v_i .

The $f_{aggregate}^{(k)}(\cdot)$ and $f_{update}^{(k)}(\cdot)$ functions in GATs are crucial. Many functions have been proposed [37]; averaging being a common aggregation method as in Eqtn. 4. We now drop k since our problem consists of a single layer.

$$\begin{aligned} \mathbf{a}_{v_i} &= \frac{1}{|\mathcal{N}_i|} \sum_{v_j \in \mathcal{N}_i} \mathbf{h}_{v_j} \\ \tilde{\mathbf{h}}_{v_i} &= f_{update}([\mathbf{h}_{v_i}, \mathbf{a}_{v_i}]) \end{aligned} \quad (4)$$

where, $[\cdot, \cdot]$ is the concatenation operation.

However, if we consider that in the first step of HOI detection, the RPN yield hundreds of proposals, then an averaging method for node features will introduce significant noise. Instead, as proposed in [31], a weighted sum is better suited to mitigate the noise. In this work, we also introduced the attention mechanism following the proposal in [31] closely. Consider a virtual node \mathbf{z}_{v_i} for a node v_i that is computed as a weighted sum over all neighbors:

$$\mathbf{z}_{v_i} = \sum_{v_j \in \mathcal{N}_i} \alpha_{ij} \mathbf{h}_{v_j} \quad (5)$$

Weights are given by:

$$\alpha_{ij} = \text{softmax}(f_{\text{attn}}(\mathbf{h}_{e_{ij}})) = \frac{\exp(f_{\text{attn}}(\mathbf{h}_{e_{ij}}))}{\sum_{v_k \in \mathcal{N}_i} \exp(f_{\text{attn}}(\mathbf{h}_{e_{ik}}))} \quad (6)$$

where, f_{attn} is a computationally efficient attention function that weighs the importance of node v_j to node v_i and can be implemented through the self-attention neural-net mechanism of [32, 33]. Its parameters are jointly learned with the target task during back propagation without additional supervision.

Once \mathbf{z}_{v_i} is computed, then an update mechanism is used to update the output feature \mathbf{h}_{v_i} . Specifics about the update will be given for the visual and semantic graphs separately in the subsequent sections.

3.3.1 Visual Graph Attention Network.

The visual graph instantiates a node v_i from the latent features \mathbf{h}_v of each of detected objects. Then, edge e_{ij} is constructed from the spatial features \mathbf{s}_{ij} from Sec. 3.2. We use an edge function $f_{\text{edge}}(\cdot)$ to integrate the features on the edge along with its two connected nodes according to:

$$\mathbf{h}_{e_{ij}} = f_{\text{edge}}([\mathbf{h}_{v_i}, \mathbf{s}_{ij}, \mathbf{h}_{v_j}]) \quad (7)$$

where, $\mathbf{h}_{e_{ij}}$ are the derived latent features for e_{ij} , with $v_j \in \mathcal{N}_i$. We then apply the the attention mechanism of Eqtn. 6 to calculate the distributions of soft weights on each edge and after which we apply a custom weighted sum:

$$\mathbf{z}_{v_i} = \sum_{v_j \in \mathcal{N}_i} \alpha_{ij} (\mathbf{h}_{v_j} \oplus \mathbf{h}_{e_{ij}}) \quad (8)$$

where, \oplus means element-wise summation operation. Note that latent feature $\mathbf{h}_{e_{ij}}$ includes the encoded relation between two nodes.

After that, we leverage a node feature updated function $f_{\text{update}}(\cdot)$ to update each node's features:

$$\tilde{\mathbf{h}}_{v_i} = f_{\text{update}}([\mathbf{h}_{v_i}, \mathbf{z}_{v_i}]) \quad (9)$$

At this point, we can get an ‘‘updated visual graph’’ with new features as illustrated in Fig. 2. The different edge thickness represent the soft weight distributions. Note that in

our method, we implement $f_{\text{attn}}(\cdot)$, $f_{\text{update}}(\cdot)$, and $f_{\text{edge}}(\cdot)$ as a single fully-connected layer network with hidden node dimensions of 1024, 1, and 1024 respectively.

3.3.2 Semantic Graph Attention Network.

In the semantic graph, Word2vec latent representations of the class labels of detected objects are used to instantiate the graph's nodes. In this graph, we do not assign any features on the edges. We denote \mathbf{w}_{v_i} as the word embedding for node i .

As with the visual graph, we use an $f'_{\text{edge}}(\cdot)$ function and an $f'_{\text{attn}}(\cdot)$ function to compute the distributions of soft weights on each edge:

$$\alpha'_{ij} = \text{softmax}(f'_{\text{attn}}(f'_{\text{edge}}([\mathbf{w}_{v_i}, \mathbf{w}_{v_j}]))) \quad (10)$$

Then, the global semantic features for each node are computed through the linear weighted sum:

$$\mathbf{z}'_{v_i} = \sum_{v_j \in \mathcal{N}_i} \alpha'_{ij} \mathbf{w}_{v_j} \quad (11)$$

After that, we update the node's features:

$$\tilde{\mathbf{w}}_{v_i} = f'_{\text{update}}([\mathbf{w}_{v_i}, \mathbf{z}'_{v_i}]) \quad (12)$$

As with the visual graph, here too, we output an ‘‘updated semantic graph’’ with new features as shown in Fig. 2. Similarly, $f'_{\text{edge}}(\cdot)$, $f'_{\text{attn}}(\cdot)$, and $f'_{\text{update}}(\cdot)$ are designed in the same way as with the visual graph.

3.4. Combined Graph.

To jointly leverage the dynamic information of both the visual (G_v) and the semantic (G_s) GATs, it is necessary to fuse them as illustrated in the ‘‘Combined Graph’’ (G_c) of Fig. 2. We concatenate the features of each of the updated nodes to produce new nodes and initialize the edges with the original spatial features described in Sec. 3.2. We denote the combined node features as γ_i for node i , where $\gamma_i = [\tilde{\mathbf{h}}_{v_i}, \tilde{\mathbf{w}}_{v_i}]$.

3.5. Readout and Inference.

The last step is to infer the interaction label for a predicate as part of our original triplet <subject, predicate, object>. Note that a person can concurrently perform different actions with each of the available target objects. That is, the subject can ‘hold’ or ‘lick’ the knife (as in Fig. 1b on the left). In effect, HOI detection is a multi-label classification problem [7]; where, each interaction class is independent and not mutually exclusive.

To simplify inference, we box-pair specific subject-object bounding boxes ($b_{h_i}, b_{o_{N_i}}$) for all \mathcal{N}_i object (nodes) directly linked to the i th human node [7, 8]. Box-pairing is illustrated in the inference section of Fig. 2.

Method	Object Detector	Full(600)↑	Rare(138)↑	Non-Rare(462)↑
InteractNet [8]	Faster R-CNN with ResNet-50-FPN	9.94	7.16	10.77
GPNN [28]	Deformable ConvNets [6]	13.11	9.34	14.23
iCAN [7]	Faster R-CNN with ResNet-50-FPN	14.84	10.45	16.15
Xu <i>et al.</i> [37]	Faster R-CNN with ResNet-50-FPN	14.70	13.26	15.13
Gupta <i>et al.</i> [12]	Faster R-CNN with ResNet-152	17.18	12.17	18.68
$RP_{T_2}C_D$ [18]	Faster R-CNN with ResNet-50-FPN	17.22	13.51	18.32
PMFNet [34]	Faster R-CNN with ResNet-50-FPN	17.46	15.65	18.00
Peyre <i>et al.</i> [26]	Faster R-CNN with ResNet-50-FPN	19.40	14.60	20.90
Ours(VS-GATs)	Faster R-CNN with ResNet-50-FPN	20.27±0.10	16.03±0.42	21.54±0.02

Table 1. mAP performance comparison with SOTA on the HICO-DET test set.

After box-pairing, we use the final human node representation γ_i , the final object node representation γ_j and mutual spatial edge features s_{ij} to form an action-specific representation $a = [\gamma_i, s_{ij}, \gamma_j]$ for prediction.

First, an action category score $\mathbf{S}_a \in \mathcal{R}^k$ where, k denotes the total number of possible actions. The computation requires an edge readout step, whose function $f_{readout}(\cdot)$ is implemented as a multi-layer perceptron². The output is then run through a binary sigmoid classifier, which produces the action score as shown in Eqtn. 13.

$$\mathbf{S}_a = \text{sigmoid}(f_{readout}(a)) \quad (13)$$

The final score of a triplet’s predicate \mathbf{S}_R can be computed through the chain multiplication of the action score \mathbf{S}_a , the detected human score s_h from object detection as well as the detected object score s_o as seen in Eqtn. 14:

$$\mathbf{S}_R = s_h * s_o * \mathbf{S}_a. \quad (14)$$

3.5.1 Training.

The overall framework is jointly optimized end-to-end, with a multi-class cross-entropy loss that is minimized between action scores and the ground truth action label:

$$\mathcal{L} = \frac{1}{N \times k} \sum_{i=1}^N \sum_{j=1}^k BCE(s_{ij}, y_{ij}^{label}) \quad (15)$$

where N is the number of all box-pairs in each mini-batch and $s_{ij} \in \mathbf{S}_a^i$. See Sec. 4.1 for more training details.

4. Experiments And Results

We evaluate the performance of VS-GATs on the HICO-DET dataset [3] and compare with the SOTA (Table 3.5.1). Ablation studies are conducted to study the impact of the proposed techniques (Table 4.3). We also visualize the

²The multi-layer perceptron consists of 2 hidden layers of dimensions 1024 and 117.

performance distribution of our model across objects for a given interaction (Fig. 3). Several detection visualization results are shown in Fig. 4.

4.1. Experimental Setup

Datasets. To evaluate HOI detection model, two common datasets are V-COCO³ [11] and HICO-DET [3]. As illustrated in [12], HICO-DET is a much larger and diverse dataset compared to V-COCO. HICO-DET consists of 38,118 training images and 9,658 testing images. The 117 interaction classes and 80 objects in HICO-DET yield 600 HOI categories in total. The dataset also has 150K annotated human-object pair instances. While V-COCO *only has 26 interactions* (a 23-fold difference) along with a training set 1/12 the size of HICO-DET’s. HICO-DET is far superior, thus making evaluations on V-COCO inconsequential. Therefore, we choose HICO-DET to evaluate our model. HICO-DET is divided into three different HOI categories: (i) Full: all 600 categories; (ii) Rare: 138 HOI categories that have less than 10 training instances, and (iii) Non-Rare: 462 HOI categories with more than 10 training instances.

Evaluation Metrics. We use the standard mean average precision (mAP) metric to evaluate the model’s detection performance. mAP is calculated with recall and precision which is common used for the detection task. In this case, we consider a detected result with the form <subject, predicate, object> is positive when the predicted verb is true and both the detected human and object bounding boxes have the intersection-of-union (IoU) exceed 0.5 with respect to the corresponding ground truth.

Implementation Details. Our architecture is built on Pytorch and the DGL library [35]. For object detection we use Pytorch’s re-implemented Faster-RCNN API [29]. Faster-RCNN use a ResNet-50-FPN backbone [14, 19] trained on the COCO dataset [20]. The object detector and Word2vec vectors are frozen during training. We keep the human bounding-boxes whose detection score exceeds 0.8, while for objects we use a 0.3 score threshold.

³We provide the results on V-COCO dataset in appendix.

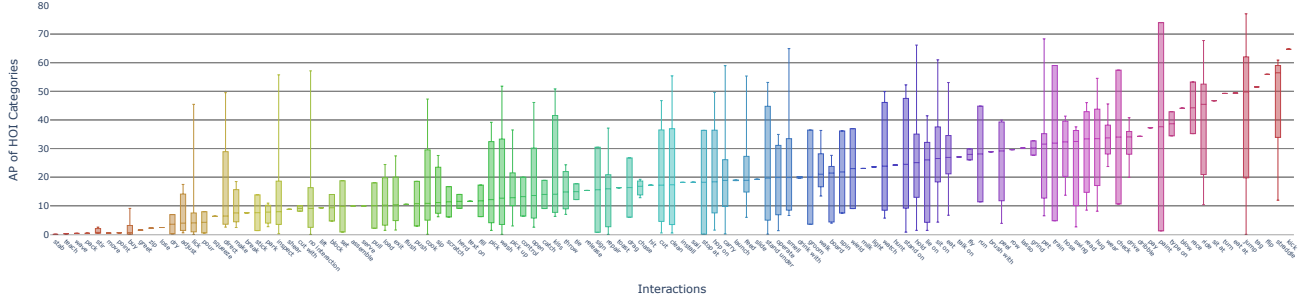


Figure 3. Spread of performance (range and quartiles) across objects for a given interaction. The horizontal axis is sorted by median AP. Plot made with open-source tool provided by [12].

For HICO-DET dataset, we first train our model on 80% (*train_set*) of training set (*trainval_set*) and validate on the other 20% (*val_set*) to perform hyperparameter selection. After fixing these parameters, we retrain on the whole training set (*trainval_set*) and report results on the *test_set*.

All neural network layers in our modal are constructed as MLPs as mentioned in previous sections. For training on HICO-DET, we use batch size of 32 and a dropout rate of 0.3. We use an Adam optimizer with a initial learning rate of $1e-5$. We reduce the learning rate to $3e-6$ at 200 epochs and stop training at 250 epochs. As for the activation function, we use a LeakyReLU in all attention network layers and a ReLU elsewhere. All experiments are conducted on a single NVIDIA TITAN RTX GPU.

4.2. Results

4.2.1 Quantitative Results and Comparisons.

Our experiments show our model achieves the best mAP results for SOTA in all three categories on HICO-DET. We achieve gains of +0.87 (4.5%) , +0.38 (2.2%) and +0.64 (3.1%) respectively.

Our multi-cue graph attention mechanism surpasses the performance of works like Peyre *et al.* [26], which exploits functional approximation through visual similarity enabling disambiguation between same-action but different-object scenarios. We also outperform works that leveraged human pose (Gupta *et al.* [12] and Wan *et al.* [34]). Pose is certainly important and plan to incorporate it in our future work. However, even without pose cues, our system still demonstrates better disambiguating power. We should also note the work of Bansal *et al.* [1] who at this time is yet unpublished but available on pre-prints. They achieve an mAP of 21.96 for the Full category and 16.43 for the Rare category. We did not include this work in our list given that they chose to pre-train their Faster-RCNN implementation directly on the HICO-DET dataset instead of COCO as the rest of the works have done. We think this gives their system an advantage compared to system that train on the more general COCO dataset. By training in this way, the

system is able to refine instance proposals and reduce uninformative instances and noise. In our work, we chose not to re-train Faster-RCNN directly on HICO-DET for fair comparison.

We hold that gains from our works are due to the multi-modal cues leveraged by the dual attention graphs. The graph structure enables the human node to leverage contextual cues from a wide-spread set of (primary and subsidiary) object instances that are dynamically updated by the independent attention mechanisms. Attention learns how—and which—contextual relations aid to disambiguate the inference. This ability is useful for the Rare category which consists of long-tail distribution samples. In conclusion, attending multi-modal cues is a powerful disambiguator. More details are presented in Sec. 4.3.

In Fig. 3, we also visualize the performance distribution of our model across objects for a given interaction. As mentioned in [12], it still holds that interactions that occur with just a single object (e.g. 'kick ball' or 'flip skateboard') are easier to detect than those predicates that interact with various objects. Compared to [12], the median AP of interaction like 'cut' and 'clean' shown in Fig. 3 outperform those in [12] by a considerable margin because our model does not only use single relation features but subsidiary ones as well.

4.2.2 Qualitative Results.

Fig. 4 shows some <subject, predicate, object> triplets' detection results on HICO-DET test dataset. From the results, our proposed model is able to detect various kinds of HOIs such as: single person-single object, multi person-same object, and multi person-multi objects.

4.3. Ablation Studies

In our ablation studies, we just train the model on the *train_set* (80% of the *trainval_set*) and directly test on the *test_set* without retraining on the *trainval_set*. We conduct six different tests to understand the performance of each of the different elements of our model. We first describe each



Figure 4. Visualization of sample HOI detections on the HICO-DET testing dataset. Subjects and objects are shown in red bounding boxes. The interaction classes are shown on the subject bounding box and the interactive objects are linked with the line in the same color. We show all triplets whose inferred *action score* (13) is greater than 0.3.

test and then analyze the results.

01 Visual Graph Only: G_V only. In this test we remove the Semantic-GAT and keep the Visual-GAT, attention, and inference the same. This study will show the importance of aggregating visual and spatial cues.

02 Semantic Graph Only: G_S only. In this test we remove the Visual-GAT and keep the Semantic-GAT, attention, and inference the same. This study will show the importance of only working with Semantic cues.

03 Without Attention. In this test, we use the averaging attention mechanism of Eqtn. 4 instead of the weighted sum mechanism. We still combine the graphs and infer in the same way.

04 Without Spatial Features in G_C . In this test, we remove spatial features from the edges of the combined graph G_C to study the role that spatial features can play after the aggregation of features across nodes.

05 Message Passing in G_C . In this test, we leverage an additional graph attention network to process the combined graph which is similar to what we do to the original visual-spatial graph. We examine if there would be a gain from an additional message passing step on G_C with combined feature from G_V and G_S .

06 Unified V-S Graph. In this test, we choose to start with a single graph in which visual and semantic features are con-

catenated in the nodes from the start. Spatial features are still used to instantiate edges. This test examines if there would be a gain from using combined visual-semantic features from the start instead of through separate streams.

Method	Full \uparrow	Rare \uparrow	Non-Rare \uparrow
Ours(VS-GATs)	19.66	15.79	20.81
01 G_V only	18.81	13.96	20.26
02 G_S only	14.61	11.76	15.46
03 w/o attention	19.01	14.12	20.47
04 w/o spatial features in G_C	18.52	14.28	19.78
05 Message passing in G_C	19.23	14.31	20.70
06 Unified V-S graph	19.39	14.84	20.75

Table 2. mAP performance for various ablation studies.

We now report on the ablation test results. For the Full category, study 01 yields an mAP of 18.81 which is a large portion of our mAP result suggesting that the visual and spatial features play a primary role in inferring HOI. When only using the Semantic graph in 02, the effect is less marked though still considerable for this single contextual semantic cue. When combining these 3 contextual cues in a graph but not using the attention mechanism in test 03, we get a gain bringing the mAP to 19.01. This

suggests that edge relations with multi-contextual cues are helpful even without attention. Afterwards, inserting attention but removing spatial features at the end in test 04 hurts. This indicates that spatial features, even after the aggregation stage, are helpful. By inserting spatial features in the combined graph we are basically using a skip connection step in neural networks which has also shown to help classification. In test 05, we learn that additional attention in the combined graph does not confer additional benefits. Rather, attention mechanisms for the independent visual-spatial and semantic features are more informative. Similarly with test 06, a combined V-S graph is still not as effective as separating cues early on. Suggesting that visual cues and semantic cues may have some degree of orthogonality to them even though they are related to each other.

5. Conclusion

In this paper we present a novel HOI detection architecture that studies and leverages the role of not only primary subject-object contextual cues in interaction, but also the role of subsidiary relations. We show that multi-modal contextual cues from visual, semantics, and spatial data can be graphically represented through graph attention networks to leverage primary and subsidiary contextual relations. Our work not only exceeds SOTA performance but excels in classifying rare categories in HICO-DET.

Appendix A: Results on V-COCO Dataset

For V-COCO dataset, we train the model with the same hyperparameter except for the dropout rate (from 0.3 to 0.5) and the training epoch (from 250 to 600). From the results, VS-GATs outperforms most of STOAAs except [34]. [34] develops a well-defined *Zoom-in Module* which utilizes *fine-grained human pose* to extract detailed local appearance cues, which make their model outperform [18] by a great margin on the small-scale dataset. However, [34] and [18] have a similar performance on the more diverse dataset HICO-DET (*HICO-DET has more fine-grained labeling of interactions (117 categories) than V-COCO (24 categories)*). Without the *Zoom-in Module*, [34] obtains the result of 48.6, which worse than our model. Moreover, the baseline of [34] also utilizes the pose cues in its spatial branch similar to [18]. However, without the expensive pose cues, VS-GATs still have a comparable performance on this small-scale dataset. We also provide the result of *ablation study 06* to support the design of our model.

Appendix B: False Positive Results

In our method, the features we leverage are visual appearance features, spatial features and the word embedding features. We think that the visual appearance features have contained the information of human pose, clothing, human

Method	AP_{role} (Sce. 1)
Gupta <i>et al.</i> [11]	31.8
InteractNet [8]	40.0
GPNN [28]	44.0
iCAN [7]	45.3
Xu <i>et al.</i> [37]	45.9
Li <i>et al.</i> ($RP_D C_D$) [18]	47.8
PMFNet Baseline [34]	48.6
PMFNet [34]	52.0
06 ablation	49.2
VS-GATs (From Scratch)	49.8
VS-GATs (+HICO-DET)	50.6

Table 3. mAP performance comparison with SOTA on the V-COCO test set. "+HICO-DET" means we first initialize the model with the learned parameters on HICO-DET before training from scratch.

gaze and so on [8]. While in some cases which need fine-grained information such as gaze detection, image depth map, human pose, temporal information, it is still hard for our model to disambiguate the interaction. The images shown in Fig. 5 are some cases which our model output the wrong detection.

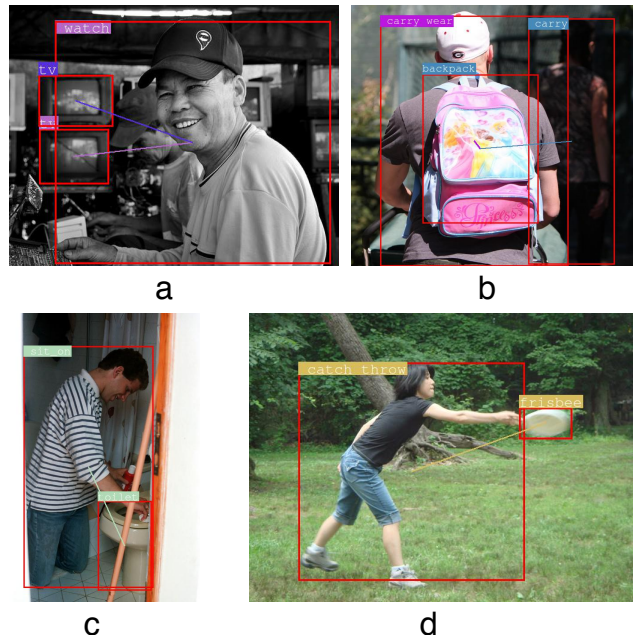


Figure 5. Visualization of some false positive HOI detections on HICO-DET testing dataset.

In image (a), it is hard to infer the right interaction in *[human-tv]* because we do not provide the model with the fine-grained gaze detection information which is the important cue to handle this situation and there seems no subsidiary relation can provides the model with significant

cues.

In image (b), our model also output the *carry* interaction between the far away *human* and the *backpack* because these two human are overlap and it seems the model need the image depth map information so that it can deal with this case better.

In image (c), our model output the wrong action *sit_on* in *[human-toilet]*. In this case, the fine-grained human pose as well as gaze detection information are helpful.

In image (d), this is an challenging case for not only the model but also human ourselves. Our model output the interactions for triplet $\langle \textit{human}, \textit{catch}, \textit{frisbee} \rangle$ and triplet $\langle \textit{human}, \textit{throw}, \textit{frisbee} \rangle$ because it is hard to distinguish them without the temporal information.

References

- [1] Ankan Bansal, Sai Saketh Rambhatla, Abhinav Shrivastava, and Rama Chellappa. Detecting Human-Object Interactions via Functional Generalization. *In arXiv preprint arXiv:1904.03181*, 2019. 2, 7
- [2] Joan Bruna, Wojciech Zaremba, Arthur Szlam, and Yann LeCun. Spectral networks and deep locally connected networks on graphs. *In ICLR*, 2014. 3
- [3] Yu-Wei Chao, Yunfan Liu, Xieyang Liu, Huayi Zeng, and Jia Deng. Learning to detect human-object interactions. *In WACV*, pages 381–389, 2018. 2, 6
- [4] Rishabh Dabral, Anurag Mundhada, Uday Kusupati, Safeer Afaq, Abhishek Sharma, and Arjun Jain. Learning 3D human pose from structure and motion. *In ECCV*, pages 668–683, 2018. 1
- [5] Jifeng Dai, Yi Li, Kaiming He, and Jian Sun. R-FCN: Object detection via region-based fully convolutional networks. *In NIPS*, pages 379–387, 2016. 1
- [6] Jifeng Dai, Haozhi Qi, Yuwen Xiong, Yi Li, Guodong Zhang, Han Hu, and Yichen Wei. Deformable Convolutional Networks. *In ICCV*, pages 764–773, 2017. 6
- [7] Chen Gao, Yuliang Zou, and Jia Bin Huang. ICAN: Instance-centric attention network for human-object interaction detection. *In BMVC*, 2018. 2, 5, 6, 9
- [8] Georgia Gkioxari, Ross Girshick, Piotr Dollár, and Kaiming He. Detecting and Recognizing Human-Object Interactions. *In CVPR*, pages 8359–8367, 2018. 2, 5, 6, 9
- [9] Google. Google Code Archive - Long-term storage for Google Code Project Hosting., 2013. 4
- [10] Marco Gori, Dipartimento Ingegneria, and Gabriele Monfardini. A New Model for Learning in Graph Domains. *In IJCNN*, 2:729–734, 2005. 3
- [11] Saurabh Gupta and Jitendra Malik. Visual semantic role labeling. *In arXiv preprint arXiv 1505.04474*, 2015. 6, 9
- [12] Tanmay Gupta, Alexander Schwing, and Derek Hoiem. No-Frills Human-Object Interaction Detection: Factorization, Layout Encodings, and Training Techniques. *In ICCV*, 2019. 2, 6, 7
- [13] Kaiming He, Georgia Gkioxari, Piotr Dollár, and Ross Girshick. Mask r-cnn. *In ICCV*, pages 2961–2969, 2017. 1
- [14] Kaiming He, Xiangyu Zhang, Shaoqing Ren, and Jian Sun. Deep residual learning for image recognition. *In CVPR*, pages 770–778, 2016. 4, 6
- [15] Ronghang Hu, Marcus Rohrbach, Jacob Andreas, Trevor Darrell, and Kate Saenko. Modeling relationships in referential expressions with compositional modular networks. *In CVPR*, pages 1115–1124, 2017. 4
- [16] Keizo Kato, Yin Li, and Abhinav Gupta. Compositional learning for human object interaction. *In ECCV*, pages 234–251, 2018. 3
- [17] Maosen Li, Siheng Chen, Xu Chen, Ya Zhang, Yanfeng Wang, and Qi Tian. Actional-Structural Graph Convolutional Networks for Skeleton-based Action Recognition. *In CVPR*, 2019. 1
- [18] Yong-Lu Li, Siyuan Zhou, Xijie Huang, Liang Xu, Ze Ma, Hao-Shu Fang, Yan-Feng Wang, and Cewu Lu. Transferable Interactiveness Knowledge for Human-Object Interaction Detection. *In CVPR*, 2018. 2, 6, 9
- [19] Tsung Yi Lin, Piotr Dollár, Ross Girshick, Kaiming He, Bharath Hariharan, and Serge Belongie. Feature pyramid networks for object detection. *In CVPR*, pages 936–944, 2017. 4, 6
- [20] Tsung Yi Lin, Michael Maire, Serge Belongie, James Hays, Pietro Perona, Deva Ramanan, Piotr Dollár, and C. Lawrence Zitnick. Microsoft COCO: Common objects in context. *In ECCV*, pages 740–755, 2014. 6
- [21] Wei Liu, Dragomir Anguelov, Dumitru Erhan, Christian Szegedy, Scott Reed, Cheng Yang Fu, and Alexander C. Berg. SSD: Single shot multibox detector. *In ECCV*, pages 21–37, 2016. 1
- [22] Cewu Lu, Ranjay Krishna, Michael Bernstein, and Li Fei-Fei. Visual relationship detection with language priors. *In ECCV*, pages 852–869, 2016. 2
- [23] Tomas Mikolov, Ilya Sutskever, Kai Chen, Greg S Corrado, and Jeff Dean. Distributed representations of words and phrases and their compositionality. *In NIPS*, pages 3111–3119, 2013. 4
- [24] Mathias Niepert, Mohamed Ahmed, and Konstantin Kutzkov. Learning convolutional neural networks for graphs. *In ICML*, pages 2014–2023, 2016. 3
- [25] Dario Pavllo, Christoph Feichtenhofer, David Grangier, and Michael Auli. 3D human pose estimation in video with temporal convolutions and semi-supervised training. *In CVPR*, pages 7753–7762, 2019. 1
- [26] Julia Peyre, Ivan Laptev, Cordelia Schmid, and Josef Sivic. Detecting unseen visual relations using analogies. *In ICCV*, pages 1981–1990, 2019. 2, 6, 7
- [27] Bryan A Plummer, Arun Mallya, Christopher M Cervantes, Julia Hockenmaier, and Svetlana Lazebnik. Phrase localization and visual relationship detection with comprehensive image-language cues. *In ICCV*, pages 1928–1937, 2017. 4
- [28] Siyuan Qi, Wenguan Wang, Baoxiong Jia, Jianbing Shen, and Song Chun Zhu. Learning human-object interactions by graph parsing neural networks. *In ECCV*, pages 407–423, 2018. 2, 3, 6, 9
- [29] Shaoqing Ren, Kaiming He, Ross Girshick, and Jian Sun. Faster R-CNN: Towards Real-Time Object Detection with

- Region Proposal Networks. *In NIPS*, pages 91–99, 2015. 1, 4, 6
- [30] Franco Scarselli, Marco Gori, Ah Chung Tsoi, Markus Hagenbuchner, and Gabriele Monfardini. Computational capabilities of graph neural networks. *IEEE Transactions on Neural Networks*, 20(1):81–102, 2008. 3
- [31] Chen Sun, Abhinav Shrivastava, Carl Vondrick, Rahul Sukthankar, Kevin Murphy, and Cordelia Schmid. Relational Action Forecasting. *In CVPR*, pages 273–283, 2019. 3, 5
- [32] Ashish Vaswani, Noam Shazeer, Niki Parmar, Jakob Uszkoreit, Llion Jones, Aidan N. Gomez, Lukasz Kaiser, and Illia Polosukhin. Attention is all you need. *In NIPS*, pages 5999–6009, 2017. 5
- [33] Petar Veličković, Arantxa Casanova, Pietro Liò, Guillem Cucurull, Adriana Romero, and Yoshua Bengio. Graph attention networks. *In ICLR*, 2018. 3, 5
- [34] Bo Wan, Desen Zhou, Yongfei Liu, Rongjie Li, and Xuming He. Pose-aware Multi-level Feature Network for Human Object Interaction Detection. *In ICCV*, pages 9469–9478, 2019. 2, 6, 7, 9
- [35] Da Zheng Quan Gan Yu Gai Zihao Ye Mufei Li Jinjing Zhou Qi Huang Chao Ma Ziyue Huang Qipeng Guo Hao Zhang Haibin Lin Junbo Zhao Jinyang Li Alexander Smola Zheng Zhang Wang Minjie, Yu Lingfan. Deep graph library: Towards efficient and scalable deep learning on graphs. *In ICLR Workshop on Representation Learning on Graphs and Manifolds*, 2019. 6
- [36] Zonghan Wu, Shirui Pan, Fengwen Chen, Guodong Long, Chengqi Zhang, and Philip S. Yu. A Comprehensive Survey on Graph Neural Networks. *Arxiv 1901.00596*, pages 1–22, 2019. 3
- [37] Bingjie Xu, Yongkang Wong, Junnan Li, Qi Zhao, and Mohan S Kankanhalli. Learning to Detect Human-Object Interactions with Knowledge. *In CVPR*, pages 2019–2028, 2019. 2, 3, 4, 6, 9
- [38] Keyulu Xu, Stefanie Jegelka, Weihua Hu, and Jure Leskovec. How powerful are graph neural networks? *In ICLR*, 2019. 4
- [39] Sijie Yan, Yuanjun Xiong, and Dahua Lin. Spatial temporal graph convolutional networks for skeleton-based action recognition. *In AAAI*, pages 7444–7452, 2018. 1
- [40] Jianwei Yang, Jiasen Lu, Stefan Lee, Dhruv Batra, and Devi Parikh. Graph R-CNN for Scene Graph Generation. *In ECCV*, pages 690–706, 2018. 3
- [41] Hanwang Zhang, Zawlin Kyaw, Shih-Fu Chang, and Tat-Seng Chua. Visual translation embedding network for visual relation detection. *In CVPR*, pages 5532–5540, 2017. 4
- [42] Bohan Zhuang, Lingqiao Liu, Chunhua Shen, and Ian Reid. Towards Context-Aware Interaction Recognition for Visual Relationship Detection. *In ICCV*, pages 589–598, 10 2017. 4